

Enhancing Perceptual Quality in Video Super-Resolution through Temporally-Consistent Detail Synthesis using Diffusion Models

Claudio Rota¹ Marco Buzzelli¹ Joost van de Weijer²

¹ University of Milano - Bicocca, Milan, Italy

² Universitat Autònoma de Barcelona, Barcelona, Spain

c.rota30@campus.unimib.it marco.buzzelli@unimib.it joost@cvc.uab.es

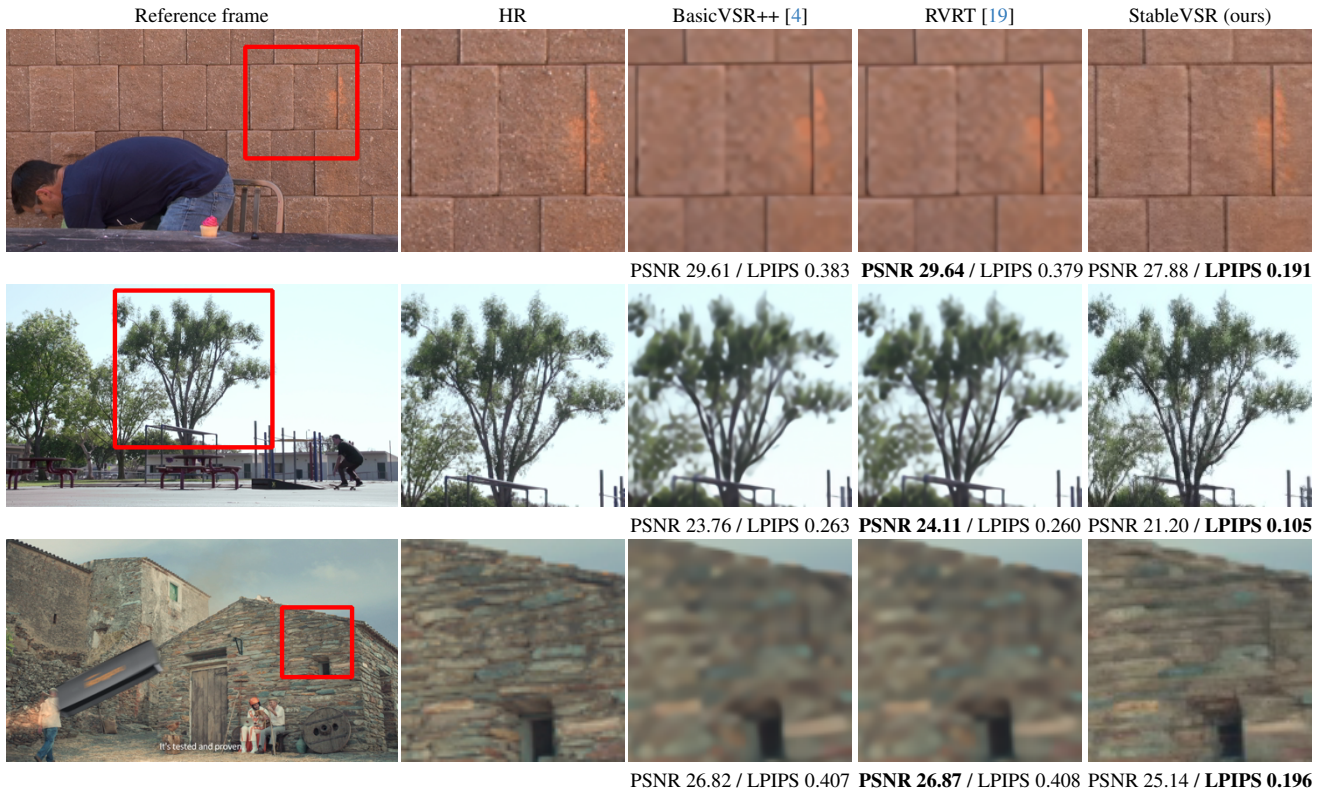


Figure 1. Reconstruction metrics, such as PSNR, only evaluate the pixel-wise difference and do not correlate well with human perception. Perceptual metrics, such as LPIPS [40], better capture the perceptual quality. The proposed StableVSR enhances the perceptual quality in video super-resolution, leading to better visual results. Best results in bold text. PSNR: the higher, the better. LPIPS [40]: the lower, the better. Results using $\times 4$ upscaling factor on Vimeo90K [37].

Abstract

In this paper, we address the problem of video super-resolution (VSR) using Diffusion Models (DM), and present StableVSR. Our method significantly enhances the perceptual quality of upscaled videos by synthesizing realistic and temporally-consistent details. We turn a pre-trained DM for single image super-resolution into a VSR

method by introducing the Temporal Conditioning Module (TCM). TCM uses Temporal Texture Guidance, which provides spatially-aligned and detail-rich texture information synthesized in adjacent frames. This guides the generative process of the current frame toward high-quality and temporally-consistent results. We introduce a Frame-wise Bidirectional Sampling strategy to encourage the use of information from past to future and vice-versa. This strategy

improves the perceptual quality of the results and the temporal consistency across frames. We demonstrate the effectiveness of StableVSR in enhancing the perceptual quality of upscaled videos compared to existing state-of-the-art methods for VSR. The code is available at <https://github.com/clauidiom4sir/StableVSR>.

1. Introduction

Video super-resolution (VSR) is the task of increasing the spatial resolution of a video by enhancing its level of detail and clarity [21]. Recently, many VSR methods based on deep learning techniques have been proposed [3, 4, 19]. However, these methods mainly focus on reconstruction quality, often ignoring perceptual quality. As a consequence, they may fail to match the fidelity expected at higher resolution [16]. According to the perception-distortion trade-off [2], improving reconstruction quality inevitably leads to a decrease in perceptual quality. As shown in Figure 1, frames generated by recent state-of-the-art methods [4, 19] have high reconstruction quality, with high PSNR values (the higher, the better), but are not perceptually photorealistic, and have high LPIPS [40] values (the lower, the better).

Inspired by the success of Diffusion Models (DMs) in generating high-quality images [6, 11, 25, 29], several works have been recently proposed to address the problem of single image super-resolution (SISR) using DMs [10, 12, 17, 30]. They show the effectiveness of DMs in synthesizing realistic textures and details, contributing to enhancing the perceptual quality of upscaled images [16]. Compared to SISR, VSR requires the integration of information from multiple closely related but misaligned frames to obtain temporal consistency over time. Unfortunately, applying frame-by-frame a SISR method to a video may lead to suboptimal results and introduces temporal inconsistency [27]. Different approaches to encourage temporal consistency in video generation using DMs have been recently studied [1, 9, 22, 38]. However, these methods do not address VSR and do not use fine-texture temporal guidance. As a consequence, they may fail to achieve temporal consistency at the fine-detail level, essential in the context of VSR.

In this paper, we address these problems and present *Stable Video Super-Resolution* (StableVSR), a novel method for VSR based on Latent Diffusion Models (LDMs) [25]. StableVSR enhances the perceptual quality of upscaled videos by synthesizing realistic and temporally-consistent details. StableVSR exploits a pre-trained LDM for SISR [25] to perform VSR by introducing the novel *Temporal Conditioning Module* (TCM). TCM guides the generative process of the current frame toward the generation of high-quality and temporally-consistent results over

time. This is achieved by using the novel *Temporal Texture Guidance*, which provides TCM with spatially-aligned and detail-rich texture information from adjacent frames: at every sampling step t , the predictions of the adjacent frames are projected to their initial state, i.e. $t = 0$, and spatially aligned to the current frame. At inference time, StableVSR uses the novel *Frame-wise Bidirectional Sampling strategy* to avoid error accumulation problems and balance information propagation: a sampling step is first taken on all frames before advancing in sampling time, and information is alternatively propagated forward and backward in video time.

In summary, our main contributions are the following:

- We present StableVSR: the first work that approaches VSR under a generative paradigm using LDMs. It significantly enhances the perceptual quality of upscaled videos while ensuring temporal consistency;
- We design *Temporal Texture Guidance* containing detail-rich and spatially-aligned texture information synthesized in adjacent frames. It guides the generative process of the current frame toward the generation of detailed and temporally consistent frames;
- We introduce *Frame-wise Bidirectional Sampling strategy* with forward and backward information propagation. It balances information propagation across frames and alleviates the problem of error accumulation;
- We quantitatively and qualitatively demonstrate the proposed StableVSR can achieve superior perceptual quality compared to existing methods for VSR.

2. Related work

Video super-resolution. Video super-resolution (VSR) based on deep learning has witnessed considerable advances in the past few years [3, 4, 18, 19, 21, 27, 32, 35]. ToFlow [37] showed that optimizing a pre-trained motion estimation method with the rest of the framework leads to better results. TDAN [32] proposed the use of deformable convolutions [42] for spatial alignment as an alternative to optical flow computation. EDVR [35] extended the alignment module proposed in TDAN [32] to better handle large motion and used temporal attention [33] to balance the contribution of each frame. BasicVSR [3] revised the essential components for a VSR method, i.e. bidirectional information propagation and spatial feature alignment, and proposed a simple yet effective solution. BasicVSR++ [4] improved BasicVSR [3] by adding second-order grid propagation and flow-guided deformable alignment. VRT [18] adopted the attention mechanism [33] to better capture long-range frame dependencies and enable parallel frame predictions. RVRT [19] improved VRT [18] by integrating the advantages of recurrent networks and reducing model complexity.

Diffusion models for single image super-resolution. The

success of Diffusion Models (DMs) in image generation [6, 11, 25, 29] inspired the development of single image super-resolution (SISR) methods based on DMs [10, 12, 17, 28, 30]. SRDiff [17] and SR3 [30] demonstrate DMs can achieve impressive results in SISR. SR3+ [28] extended SR3 [30] to images in the wild by proposing a higher-order degradation scheme and noise conditioning augmentation. LDM [25] proposed to work in a VAE latent space [8] to reduce complexity requirements and training time. CMD [12] proposed to cascade multiple DMs to achieve SISR at arbitrary scales. IDM [10] proposed to introduce the implicit image function in the decoding part of a DM to achieve continuous super-resolution.

3. Background on Diffusion Models

Diffusion Models (DMs) [11] convert a complex data distribution $x_0 \sim p_{data}$ into a simple Gaussian distribution $x_T \sim \mathcal{N}(0, I)$, and then recover data from it. A DM is composed of two processes: diffusion process and reverse process.

Diffusion process. The diffusion process is a Markov chain that corrupts data $x_0 \sim p_{data}$ until they approach Gaussian noise $x_T \sim \mathcal{N}(0, I)$ after T diffusion steps. It is defined as:

$$q(x_1, \dots, x_T | x_0) = \prod_{t=1}^T q(x_t | x_{t-1}) \quad (1)$$

where t represents a diffusion step and $q(x_t | x_{t-1}) = \mathcal{N}(x_t; \sqrt{1 - \beta_t}(x_{t-1}), \beta_t I)$, with β_t being a fixed or learnable variance schedule. At any step t , x_t can be directly sampled from x_0 as:

$$x_t = \sqrt{\bar{\alpha}_t} x_0 + \sqrt{1 - \bar{\alpha}_t} \epsilon \quad (2)$$

where $\alpha_t = 1 - \beta_t$, $\bar{\alpha}_t = \prod_{i=1}^t \alpha_i$ and $\epsilon \sim \mathcal{N}(0, I)$.

Reverse process. The reverse process is a Markov chain that removes noise from $x_T \sim \mathcal{N}(0, I)$ until data $x_0 \sim p_{data}$ are obtained. It is defined as:

$$p_\theta(x_0, \dots, x_{T-1} | x_T) = \prod_{t=1}^T p_\theta(x_{t-1} | x_t) \quad (3)$$

where $p_\theta(x_{t-1} | x_t) = \mathcal{N}(x_{t-1}; \mu_\theta(x_t, t), \Sigma_\theta I)$. A neural network ϵ_θ is trained to predict ϵ from x_t , and it can be used to estimate $\mu_\theta(x_t, t)$ as:

$$\mu_\theta(x_t, t) = \frac{1}{\sqrt{\alpha_t}} \left(x_t - \frac{1 - \alpha_t}{\sqrt{1 - \bar{\alpha}_t}} \epsilon_\theta(x_t, t) \right) \quad (4)$$

As a consequence, we can sample $x_{t-1} \sim p_\theta(x_{t-1} | x_t)$ as:

$$x_{t-1} = \frac{1}{\sqrt{\alpha_t}} \left(x_t - \frac{1 - \alpha_t}{\sqrt{1 - \bar{\alpha}_t}} \epsilon_\theta(x_t, t) \right) + \sigma_t z \quad (5)$$

where $z \sim \mathcal{N}(0, I)$ and σ_t is the variance schedule. In practice, according to Eq. 2, we can directly predict \tilde{x}_0 from x_t via projection to the initial state $t = 0$ as:

$$\tilde{x}_0 = \frac{1}{\sqrt{\bar{\alpha}_t}} \left(x_t - \sqrt{1 - \bar{\alpha}_t} \epsilon_\theta(x_t, t) \right) \quad (6)$$

and then sample x_{t-1} using x_0 and x_t as:

$$x_{t-1} = \frac{\sqrt{\bar{\alpha}_{t-1}}(1 - \alpha_t)}{1 - \bar{\alpha}_t} \tilde{x}_0 + \frac{\sqrt{\alpha_t}(1 - \bar{\alpha}_{t-1})}{1 - \bar{\alpha}_t} x_t + \sigma_t z \quad (7)$$

where $z \sim \mathcal{N}(0, I)$ and σ_t is the variance schedule.

4. Methodology

We present Stable Video Super-Resolution (StableVSR), a method for video super-resolution (VSR) based on Latent Diffusion Models (LDM) [25]. StableVSR enhances the perceptual quality in VSR through temporally-consistent detail synthesis. The overview of the method is shown in Figure 2. StableVSR is built upon a pre-trained LDM for single image super-resolution [25], which is turned into a VSR method through the design and addition of the Temporal Conditioning Module (TCM). TCM uses detail and structure information synthesized in adjacent frames to guide the generative process of the current frame. It allows to obtain high-quality and temporally-consistent frames over time. We design the Temporal Texture Guidance to provide TCM with rich texture information about the adjacent frames: at every sampling step, their predictions are projected to their initial state via Eq. 6, converted into RGB frames, and aligned with the current frame via optical flow estimation and motion compensation. We introduce in StableVSR the Frame-wise Bidirectional Sampling strategy, where a sampling step is taken on all frames advancing in sampling time, and information is alternatively propagated forward and backward in video time. This alleviates the problem of error accumulation and balances the information propagation over time.

4.1. Temporal Conditioning Module

Applying frame-by-frame the SISR LDM [25] to videos introduces temporal inconsistency, as each frame is generated only based on the content of a single low-resolution frame. Moreover, this approach does not exploit the content shared among multiple video frames, leading to sub-optimal results [27]. We address these problems by introducing the Temporal Conditioning Module (TCM) into the SISR LDM [25]. The goal is twofold: (1) enabling the use of spatio-temporal information from multiple frames; (2) enforcing temporal consistency across frames. We use the information generated by the SISR LDM [25] in the adjacent frames to guide the generation process of the current

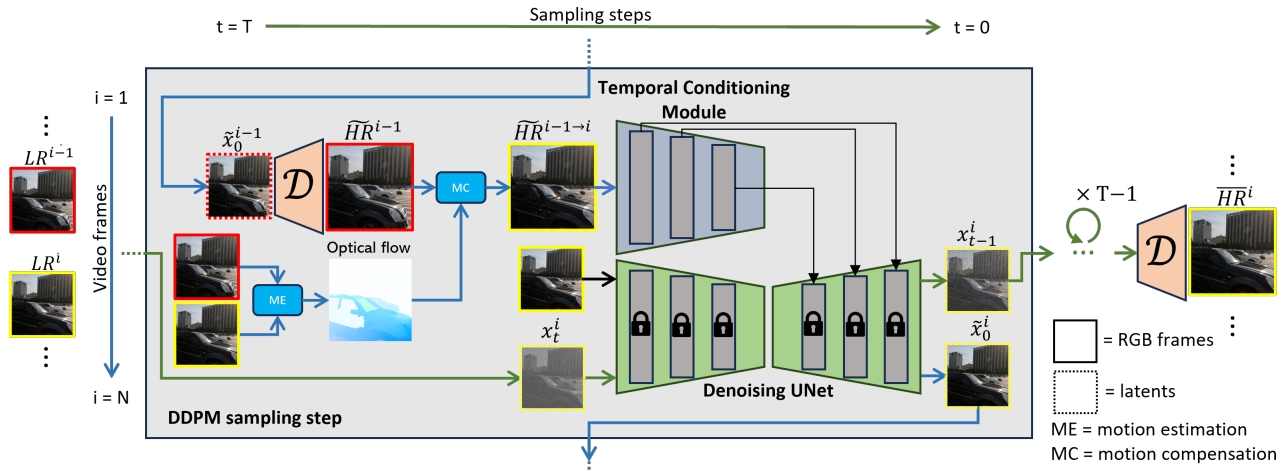


Figure 2. Overview of the proposed StableVSR. We turn a single image super-resolution LDM [25] into a video super-resolution method through the Temporal Conditioning Module (TCM) (Section 4.1). TCM exploits the Temporal Texture Guidance $\widetilde{HR}^{i-1 \rightarrow i}$ (Section 4.2). It provides TCM with spatially-aligned and detail-rich texture information synthesized in adjacent frames to guide the generative process of the current frame toward detail-rich and temporally-consistent results over time. The sampling step is taken using the Frame-wise Bidirectional Sampling strategy (Section 4.3). \mathcal{D} represents the VAE decoder [8]. Green lines refer to progression in sampling time, while blue lines refer to progression in video time.

frame. Besides obtaining temporal consistency, this solution also provides additional sources of information to handle very small or occluded objects. TCM injects temporal conditioning into the decoder of the denoising UNet [26], as proposed in ControlNet [39].

4.2. Temporal Texture Guidance

The Temporal Texture Guidance provides the Temporal Conditioning Module with the texture information synthesized in adjacent frames. The goal is to guide the generative process of the current frame toward the generation of high-quality and temporally-consistent results.

Guidance on \tilde{x}_0 . Using results of the previous sampling step $\{x_t\}_{i=1}^N$ as guidance to predict $\{x_{t-1}\}_{i=1}^N$, as proposed in [1, 22], may not provide adequate texture information along the whole reverse process. This is because x_t is corrupted by noise until t approaches 0, as shown in Figure 3. We address this problem by using a noise-free approximation of x_t , i.e. \tilde{x}_0 , to be used as guidance when taking a given sampling step t . This is achieved by projecting x_t to its initial state, i.e. $t = 0$, using Eq 6. Since $\tilde{x}_0 \approx x_0$, it contains very little noise. In addition, it provides detail-rich texture information that is gradually refined as t approaches 0, as shown in Figure 3.

Temporal conditioning. We need to use information synthesized in adjacent frames to ensure temporal consistency. We achieve this by using \tilde{x}_0 obtained from the previous frame, i.e. \tilde{x}_0^{i-1} , as guidance when generating the current frame. Since \tilde{x}_0^{i-1} is computed from x_t^{i-1} using

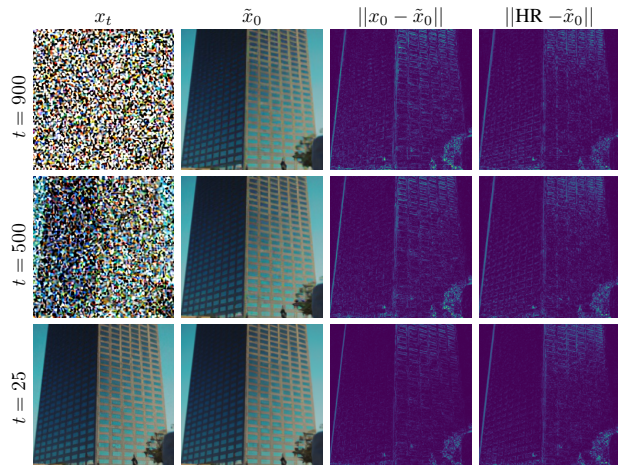


Figure 3. Comparison between guidance on x_t and \tilde{x}_0 . Compared to x_t (first column), \tilde{x}_0 computed via Eq. 6 contains very little noise regardless of the sampling step t (second column). We can observe \tilde{x}_0 is closer to x_0 as t decreases (third column). Here, x_0 corresponds to the last sampling step, i.e. when $t = 1$. In addition, \tilde{x}_0 increases its level of detail as t decreases (fourth column).

$\epsilon_{\theta}(x_t^{i-1}, t, LR^{i-1})$ via Eq. 6, it contains the texture information synthesized in the previous frame at sampling step t .

Spatial alignment. According to [3], spatial alignment is essential to properly aggregate information from multiple frames. The texture information contained in \tilde{x}_0^{i-1} may not be spatially aligned with respect to the current frame due to

Motion compensation applied to \tilde{x}_0 Motion compensation applied to $\mathcal{D}(\tilde{x}_0)$

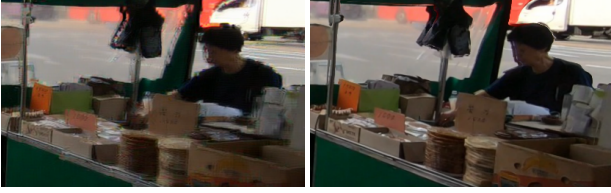


Figure 4. Comparison between applying motion compensation to \tilde{x}_0 in the latent space and to $\mathcal{D}(\tilde{x}_0)$ in the pixel domain. \mathcal{D} represents the VAE decoder [8]. In the first scenario, visible artifacts are introduced.

video motion. We achieve spatial alignment via motion estimation and compensation, computing optical flow on the respective low-resolution frames LR^{i-1} and LR^i . Directly applying motion compensation to \tilde{x}_0^{i-1} in the latent space introduces artifacts, as shown in Figure 4. We address this problem by converting \tilde{x}_0^{i-1} from the latent space to the pixel domain through the VAE decoder \mathcal{D} [8] and then applying motion compensation.

Formulation. Given the previous and the current low-resolution frames LR^{i-1} and LR^i , the current sampling step t and the latent of the previous frame x_t^{i-1} , the Temporal Texture Guidance $\widetilde{\text{HR}}^{i-1 \rightarrow i}$ is computed as:

$$\widetilde{\text{HR}}^{i-1 \rightarrow i} = \text{MC}(\text{ME}(\text{LR}^{i-1}, \text{LR}^i), \mathcal{D}(\tilde{x}_0^{i-1})) \quad (8)$$

where MC is the motion compensation function, ME is the motion estimation method, \mathcal{D} is the VAE decoder [8] and \tilde{x}_0^{i-1} is computed via Eq. 6 using $\epsilon_\theta(x_t^{i-1}, t, \text{LR}^{i-1})$.

4.3. Frame-wise Bidirectional Sampling strategy

Progressing all the sampling steps on one frame and using the result as guidance for the next frame in an autoregressive manner, as proposed in [38], may introduce the problem of error accumulation. In addition, unidirectional information propagation from past to future frames may lead to suboptimal results [3]. We address these problems by proposing the Frame-wise Bidirectional Sampling strategy: we take a given sampling step t on all the frames before taking the next sampling step $t-1$, alternatively propagating information forward and backward in video time. The pseudocode is detailed in Algorithm 1. Given the latent x_t^i at a sampling step t , the Temporal Texture Guidance $\widetilde{\text{HR}}^{i-1 \rightarrow i}$ used by the Temporal Conditioning Module is alternatively computed via Eq. 8 using \tilde{x}_0^{i-1} or \tilde{x}_0^{i+1} , respectively related to the previous or the next frame. Information is propagated forward and backward in video time: the current frame is conditioned by past frames during forward propagation, and by future frames during backward propagation. The first and the last frames of the sequence do

Algorithm 1 Frame-wise Bidirectional Sampling strategy. ME and MC are “motion estimation” and “motion compensation”, respectively.

Input: Sequence of low-resolution frames $\{\text{LR}\}^N$; pre-trained ϵ_θ for VSR, VAE decoder \mathcal{D} ; method for ME.

- 1: **for** $i = 1$ to N **do**
- 2: $x_T^i = \mathcal{N}(0, I)$
- 3: **end for**
- 4: **for** $t = T$ to 1 **do**
- 5: **for** $i = 1$ to N **do** ▷ Take a given sampling step on all the frames
- 6: $\widetilde{\text{HR}}^{i-1 \rightarrow i} = \text{MC}(\text{ME}(\text{LR}^{i-1}, \text{LR}^i), \mathcal{D}(\tilde{x}_0^{i-1}))$ **if** $i > 1$ ▷ Eq. 8
- 7: $\tilde{\epsilon} = \epsilon_\theta(x_t^i, t, \text{LR}^i, \widetilde{\text{HR}}^{i-1 \rightarrow i})$ **if** $i > 1$ **else** $\epsilon_\theta(x_t^i, t, \text{LR}^i)$
- 8: $\tilde{x}_0^i = \frac{1}{\sqrt{\alpha_t}} (x_t^i - \sqrt{1 - \alpha_t} \tilde{\epsilon})$ ▷ Eq. 6
- 9: $z = \mathcal{N}(0, I)$ **if** $t > 1$ **else** 0
- 10: $x_{t-1}^i = \frac{1}{\sqrt{\alpha_t}} \left(x_t^i - \frac{1 - \alpha_t}{\sqrt{1 - \alpha_t}} \tilde{\epsilon} \right) + \sigma_t z$ ▷ Eq. 5
- 11: **end for**
- 12: Reverse sequence order of $\{x_{t-1}\}^N$, $\{\tilde{x}_0\}^N$ and $\{\text{LR}\}^N$
- 13: **end for**
- 14: **return** $\{\widetilde{\text{HR}}\}^N = \{\mathcal{D}(x_0)\}^N$

Algorithm 2 Training procedure. ME and MC are “motion estimation” and “motion compensation”, respectively.

Input: Dataset D with (LR, HR) pairs; pre-trained ϵ_θ for SISR, method for ME.

- 1: **repeat**
- 2: $(\text{LR}^{i-1}, \text{HR}^{i-1}), (\text{LR}^i, \text{HR}^i) \sim D$
- 3: $x_0^{i-1}, x_0^i = \mathcal{E}(\text{HR}^{i-1}), \mathcal{E}(\text{HR}^i)$
- 4: $\epsilon^{i-1}, \epsilon^i \sim \mathcal{N}(0, I)$
- 5: $t \sim \{0, \dots, T\}$
- 6: $\tilde{\epsilon}^{i-1} = \epsilon_\theta(\sqrt{\alpha_t} x_0^{i-1} + \sqrt{1 - \alpha_t} \epsilon^{i-1}, t, \text{LR}^{i-1})$
- 7: $\tilde{x}_0^{i-1} = \frac{1}{\sqrt{\alpha_t}} (x_0^{i-1} - \sqrt{1 - \alpha_t} \tilde{\epsilon}^{i-1})$ ▷ Eq. 6
- 8: $\widetilde{\text{HR}}^{i-1 \rightarrow i} = \text{MC}(\text{ME}(\text{LR}^{i-1}, \text{LR}^i), \mathcal{D}(\tilde{x}_0^{i-1}))$ ▷ Eq. 8
- 9: Take gradient descent step on:
- 10: $\nabla_\theta (||\epsilon^i - \epsilon_\theta(\sqrt{\alpha_t} x_0^i + \sqrt{1 - \alpha_t} \epsilon^i, t, \text{LR}^i, \widetilde{\text{HR}}^{i-1 \rightarrow i})||)$
- 11: **until** convergence

not use the Temporal Conditioning Module during forward and backward propagation, respectively. This is in line with other methods [3, 4].

4.4. Training procedure

StableVSR is built upon a pre-trained LDM for single image super-resolution [25], hence we only need to train the Temporal Conditioning Module. We extend the ControlNet [39] training procedure by adding an additional step to compute the Temporal Texture Guidance $\widetilde{\text{HR}}^{i-1 \rightarrow i}$ from the previous frame to be used for the current one. The pseudocode is detailed in Algorithm 2. Given two (LR, HR) pairs of consecutive frames $(\text{LR}^{i-1}, \text{HR}^{i-1})$ and $(\text{LR}^i, \text{HR}^i)$, we first compute x_0^{i-1} and x_0^i by converting HR^{i-1} and HR^i into the latent space using the VAE encoder \mathcal{E} [8]. We add $\epsilon \sim \mathcal{N}(0, I)$ to x_0^{i-1} via Eq. 2, obtaining x_t^{i-1} . We then compute \tilde{x}_0^{i-1} using x_t^{i-1} and $\epsilon_\theta(x_t^{i-1}, t, \text{LR}^{i-1})$ via Eq. 6, and we obtain $\widetilde{\text{HR}}^{i-1 \rightarrow i}$ to be used for the current frame via Eq. 8. The training objective is:

$$\mathbb{E}_{t, x_0^i, \epsilon, \text{LR}^i, \widetilde{\text{HR}}^{i-1 \rightarrow i}} [||\epsilon - \epsilon_\theta(x_t^i, t, \text{LR}^i, \widetilde{\text{HR}}^{i-1 \rightarrow i})||], \quad (9)$$

Table 1. Quantitative comparison with state-of-art methods. Perceptual metrics are marked with \star and reconstruction metrics with \diamond . Best results in bold text. All the perceptual metrics highlight the proposed StableVSR achieves better perceptual quality.

	Vimeo-90K [37]								REDS [24]					
	LPIPS \star \downarrow	DISTS \star \downarrow	MUSIQ \star \uparrow	CLIP-IQA \star \uparrow	NIQE \star \downarrow	PSNR \diamond \uparrow	SSIM \diamond \uparrow	LPIPS \star \downarrow	DISTS \star \downarrow	MUSIQ \star \uparrow	CLIP-IQA \star \uparrow	NIQE \star \downarrow	PSNR \diamond \uparrow	SSIM \diamond \uparrow
Bicubic	0.289	0.209	23.27	0.358	8.44	29.75	0.848	0.453	0.186	26.89	0.304	6.85	26.13	0.729
ToFlow [37]	0.152	0.150	40.79	0.364	8.05	32.28	0.898	-	-	-	-	-	-	-
EDVR [35]	-	-	-	-	-	-	-	0.178	0.082	65.44	0.367	4.15	31.02	0.879
TDAN [32]	0.120	0.122	46.54	0.386	7.34	34.10	0.919	-	-	-	-	-	-	-
BasicVSR [3]	0.103	0.113	48.97	0.376	7.27	35.18	0.931	0.165	0.081	65.74	0.371	4.06	31.39	0.891
VRT [18]	0.084	0.100	51.08	0.389	7.11	36.35	0.942	0.173	0.081	65.68	0.374	4.19	31.59	0.889
BasicVSR++ [4]	0.092	0.105	50.11	0.383	7.12	35.69	0.937	0.131	0.068	67.00	0.381	3.87	32.38	0.907
RVRT [19]	0.088	0.101	50.45	0.387	7.12	36.30	0.942	0.128	0.067	67.44	0.392	3.78	32.74	0.911
StableVSR (Ours)	0.070	0.087	50.97	0.414	5.99	31.97	0.877	0.097	0.045	67.54	0.417	2.73	27.97	0.800

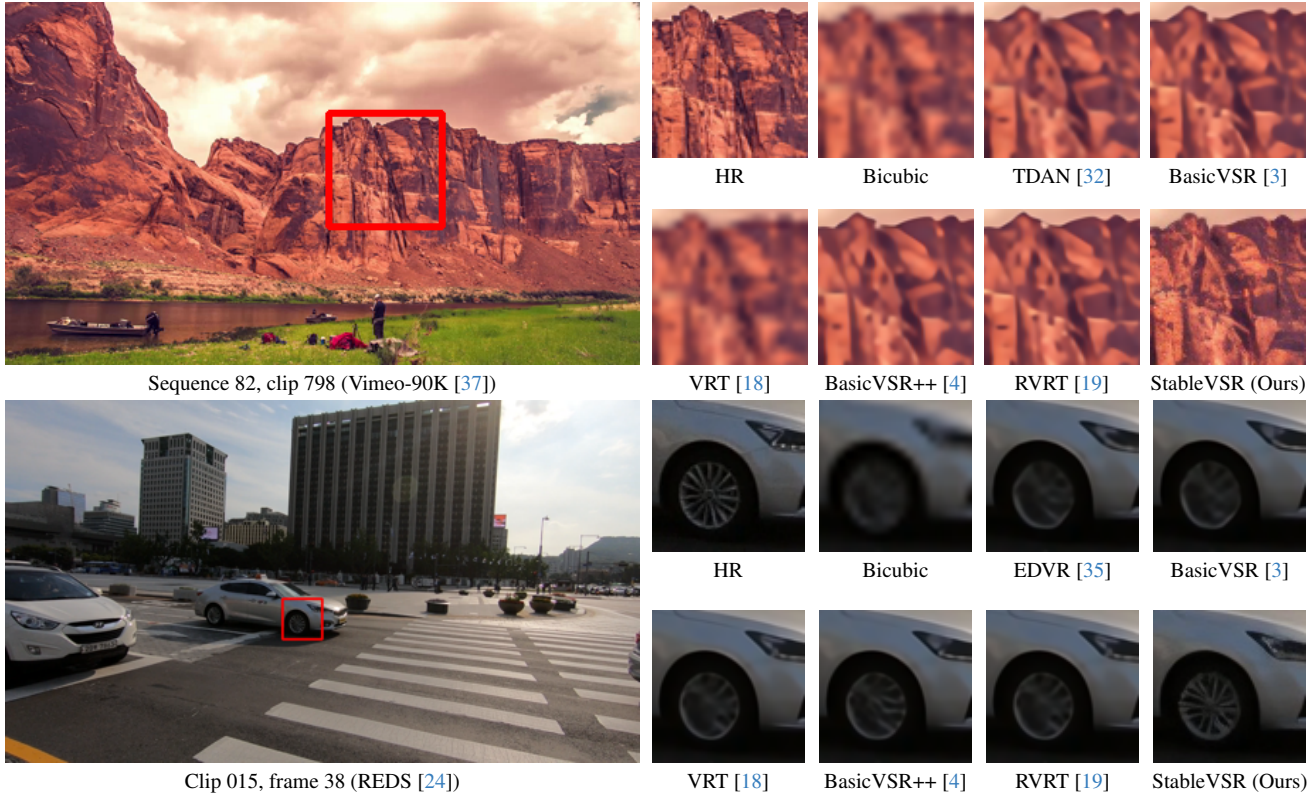


Figure 5. Qualitative comparison with state-of-the-art methods for VSR. The proposed StableVSR better enhances the perceptual quality of the upscaled frames by synthesizing more realistic details.

where $t \sim [1, T]$ and x_t^i is obtained by adding $\epsilon \sim \mathcal{N}(0, I)$ to x_0^i via Eq. 2.

5. Experiments

5.1. Implementation details

StableVSR is built upon Stable Diffusion $\times 4$ upscaler¹ (SD $\times 4$ Upscaler) [25], which uses the low-resolution images as guidance via concatenation. SD $\times 4$ Upscaler uses a VAE decoder [8] with $\times 4$ upscaling factor to perform super-resolution. We use the same decoder in our StableVSR. The

¹<https://huggingface.co/stabilityai/stable-diffusion-x4-upscaler>

architecture details are reported in the supplementary material. In all our experiments, the results are referred to $\times 4$ super-resolution. We add the Temporal Conditioning Module via ControlNet [39] and train it for 20000 steps. We use RAFT [31] for optical flow computation. We use 4 NVIDIA Quadro RTX 6000 for our experiments. We use the Adam optimizer [14] with a batch size set to 32 and the learning rate fixed to $1e - 5$. Randomly cropped patches of size 256×256 with horizontal flip are used as data augmentation. We use DDPM [11] sampling with $T = 1000$ during training and $T = 50$ during inference.

5.2. Datasets and evaluation metrics

We adopt two benchmark datasets: Vimeo-90K [37] and REDS [24]. Vimeo-90K [37] contains 91701 7-frame video sequences at 448×256 resolution. It covers a broad range of actions and scenes. Among these sequences, 64612 are used for training and 7824 for testing. REDS [24] is a realistic and dynamic scene dataset containing 300 video sequences. Each sequence has 100 frames at 1280×720 resolution. Following previous work [3, 4], we use sequences 000, 011, 015, and 020 for testing and all the others for training. We use a variety of perceptual metrics, including LPIPS [40], DISTS [7], MUSIQ [13], CLIP-IQA [34] and NIQE [23], to evaluate the perceptual quality of StableVSR results. We also report reconstruction metrics like PSNR and SSIM [36] for reference. We adopt Warping Error (WE) [15] for the evaluation of temporal consistency. MUSIQ [13], CLIP-IQA [34] and NIQE [23] are no-reference metrics, while LPIPS [40], DISTS [7], PSNR, SSIM [36] and WE [15] are full-reference metrics.

5.3. Comparison with state-of-the-art methods

We compare StableVSR with other state-of-the-art methods including ToFlow [37], EDVR [35], TDAN [32], BasicVSR [3], VRT [18] BasicVSR++ [4] and RVRT [19]. Since only PSNR and SSIM [36] are evaluated in the official papers, we use the results obtained using the pre-trained models to evaluate the other metrics. The quantitative comparison is reported in Table 1. As shown, StableVSR outperforms the other methods considering all the perceptual metrics. This is also confirmed by the qualitative results shown in Figure 5: the frames upscaled by StableVSR look more natural and realistic. StableVSR, due to its generative nature, is the only method able to synthesize information that cannot be found in the spatio-temporal frame neighborhood. This is because it captures the semantics of the scenes and synthesizes missing information accordingly. In Table 1, we can observe StableVSR has poorer performance in PSNR and SSIM [36]. This is in line with the perception-distortion trade-off [2]. We report additional results in the supplementary material.

5.4. Impact of sampling steps

We study how the performance changes as the number of sampling steps increases. Figure 6 shows the results obtained by increasing the number of sampling steps from 10 to 100. Reconstruction quality (PSNR and SSIM [36]) deteriorates with more sampling steps. Conversely, perceptual quality (LPIPS [40], DISTS [7], MUSIQ [13], CLIP-IQA [34] and NIQE [23]) improves. We can attribute this behavior to the iterative refinement process of Diffusion Models, which progressively refines realistic image details that may not be perfectly aligned with the reference. In addition, since frames obtained using very few steps are

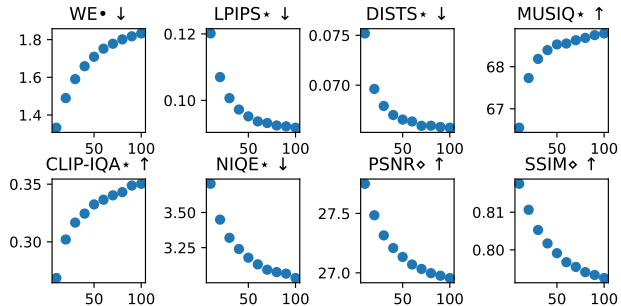


Figure 6. Performance changes as the number of sampling steps increases. The x axis represents sampling steps, while the y axis metric values. Perceptual metrics are marked with \star , reconstruction metrics with \diamond , and temporal consistency metrics with \bullet . Increasing the sampling steps improves perceptual quality while deteriorating reconstruction quality and temporal consistency. Results computed on center crops of 512×512 target resolution of REDS [24].

Table 2. Quantitative comparison of different sampling strategies. Perceptual metrics are marked with \star , reconstruction metrics with \diamond , and temporal consistency metrics with \bullet . Best results in bold text. Here we only report full-reference metrics. We can see the proposed Frame-wise Bidirectional Sampling strategy leads to better results.

	WE \bullet ↓	LPIPS \star ↓	DISTS \star ↓	PSNR \diamond ↑	SSIM \diamond ↑
Single-frame	2.44	0.121	0.055	26.32	0.732
Auto-regressive	1.60	0.119	0.059	26.48	0.743
Unidirectional	1.57	0.100	0.047	27.74	0.788
Bidirectional	1.51	0.097	0.045	27.97	0.800

blurry, the temporal consistency measured via WE [15] is higher. According to these results, 50 sampling steps represent a good balance between perceptual quality and temporal consistency.

5.5. Ablation study

Temporal Texture Guidance. Figure 7 shows the results obtained by removing one of the operations in the Temporal Texture Guidance. Using guidance on x_t instead of \tilde{x}_0 leads to very noisy frames. These noisy frames cannot provide adequate information when t is far from 0. With no motion compensation, the spatial information is not aligned with respect to the current frame and cannot be properly used. Applying motion compensation in the latent space introduces distortions in the guidance, as also shown in Figure 4. In all these cases, temporal consistency at fine-detail level cannot be achieved. The proposed approach provides detail-rich and spatially-aligned texture guidance at every sampling step t , leading to better temporal consistency.

Frame-wise Bidirectional Sampling strategy. We compare the proposed Frame-wise Bidirectional Sampling strat-



Figure 7. Ablation experiments for the Temporal Texture Guidance. Only the proposed solution can provide detail-rich and spatially-aligned texture information from adjacent frames at every sampling step t . MC refers to “motion compensation”. For “No guidance on \tilde{x}_0 ” experiment, we use guidance on x_t . For “No Latent \rightarrow RGB conversion” experiment, the aligned latent is converted to RGB just for visualization.

egy with: single-frame sampling, i.e. no temporal conditioning; auto-regressive sampling, i.e. the previous up-scaled frame is used as guidance for the current one; frame-wise unidirectional sampling, i.e. only forward information propagation. The results are quantitatively and qualitatively evaluated in Table 2 and Figure 8, respectively. Single-frame sampling leads to poor results and introduces temporal inconsistency due to the differences in the synthesized frame details. The auto-regressive approach has the problem of error accumulation, which is propagated to the next frames. Unidirectional sampling unbalances the information propagation, as only future frames receive information from the past ones, limiting the overall performance. The proposed Frame-wise Bidirectional Sampling solves these problems, leading to better and more consistent results.

6. Discussion and limitations

Reconstruction quality results. We focus on using Diffusion Models (DMs) to enhance the perceptual quality in video super-resolution (VSR). Improving perceptual quality inevitably leads to a decrease in reconstruction quality [2]. Recent works on single image super-resolution using DMs [10, 17, 30] reported lower reconstruction quality when compared to regression-based methods [5, 20].

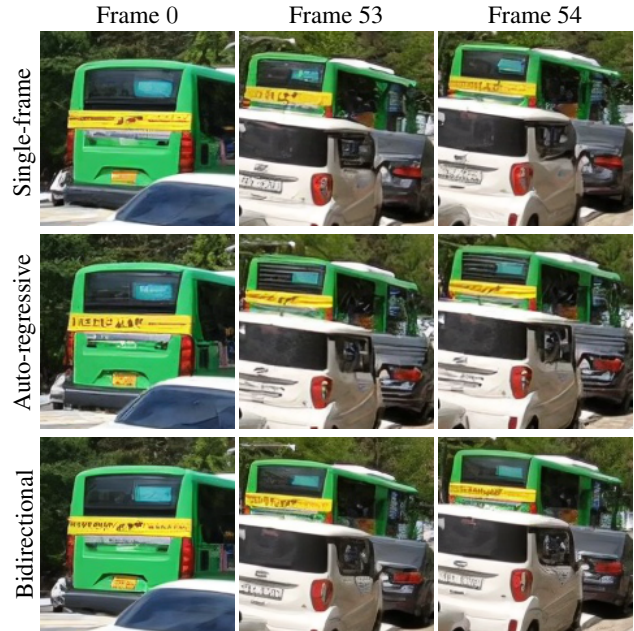


Figure 8. Qualitative comparison of different sampling strategies. Single-frame sampling introduces temporal inconsistency. Auto-regressive sampling shows the error accumulation problem. The proposed bidirectional propagation solves both the problems.

Although most VSR methods target reconstruction quality, several studies [21, 27] highlighted the urgent need to address perceptual quality. We take a step in this direction.

Model complexity. The complexity of the denoising UNet [26] we use in StableVSR is $\times 20$ higher than the compared methods, increasing training time and memory occupation requirements. The iterative refinement process of DMs inevitably increases inference time. StableVSR takes about 100 seconds to upscale a video to a 1280×720 target resolution on a NVIDIA Quadro RTX A6000 using 50 sampling steps. In future works, we plan to incorporate current research in speeding up DMs [41].

7. Conclusions

We proposed to enhance the perceptual quality in video super-resolution (VSR) through the synthesis of temporally-consistent details using Diffusion Models (DMs), and presented StableVSR. We turned a pre-trained DM for single-image super-resolution into a VSR method by introducing a Temporal Conditioning Module (TCM). It uses Temporal Texture Guidance with spatially-aligned and detail-rich texture information from adjacent frames to guide the generative process of the current frame toward the generation of high-quality results and ensure temporal consistency. We adopted a Frame-wise Bidirectional Sampling strategy at inference time to further improve percep-

tual quality and temporal consistency. We compared StableVSR with existing state-of-the-art methods for VSR, and showed that it better enhances the perceptual quality of up-scaled frames both quantitatively and qualitatively.

References

- [1] Andreas Blattmann, Robin Rombach, Huan Ling, Tim Dockhorn, Seung Wook Kim, Sanja Fidler, and Karsten Kreis. Align your latents: High-resolution video synthesis with latent diffusion models. In *Proceedings of the IEEE/CVF Conference on Computer Vision and Pattern Recognition*, pages 22563–22575, 2023. [2](#), [4](#)
- [2] Yochai Blau and Tomer Michaeli. The perception-distortion tradeoff. In *Proceedings of the IEEE conference on computer vision and pattern recognition*, pages 6228–6237, 2018. [2](#), [7](#), [8](#)
- [3] Kelvin CK Chan, Xintao Wang, Ke Yu, Chao Dong, and Chen Change Loy. Basicvsr: The search for essential components in video super-resolution and beyond. In *Proceedings of the IEEE/CVF conference on computer vision and pattern recognition*, pages 4947–4956, 2021. [2](#), [4](#), [5](#), [6](#), [7](#)
- [4] Kelvin CK Chan, Shangchen Zhou, Xiangyu Xu, and Chen Change Loy. Basicvsr++: Improving video super-resolution with enhanced propagation and alignment. In *Proceedings of the IEEE/CVF conference on computer vision and pattern recognition*, pages 5972–5981, 2022. [1](#), [2](#), [5](#), [6](#), [7](#)
- [5] Yinbo Chen, Sifei Liu, and Xiaolong Wang. Learning continuous image representation with local implicit image function. In *Proceedings of the IEEE/CVF conference on computer vision and pattern recognition*, pages 8628–8638, 2021. [8](#)
- [6] Prafulla Dhariwal and Alexander Nichol. Diffusion models beat gans on image synthesis. *Advances in neural information processing systems*, 34:8780–8794, 2021. [2](#), [3](#)
- [7] Keyan Ding, Kede Ma, Shiqi Wang, and Eero P Simoncelli. Image quality assessment: Unifying structure and texture similarity. *IEEE transactions on pattern analysis and machine intelligence*, 44(5):2567–2581, 2020. [7](#)
- [8] Patrick Esser, Robin Rombach, and Bjorn Ommer. Taming transformers for high-resolution image synthesis. In *Proceedings of the IEEE/CVF conference on computer vision and pattern recognition*, pages 12873–12883, 2021. [3](#), [4](#), [5](#), [6](#), [1](#)
- [9] Patrick Esser, Johnathan Chiu, Parmida Atighehchian, Jonathan Granskog, and Anastasis Germanidis. Structure and content-guided video synthesis with diffusion models. In *Proceedings of the IEEE/CVF International Conference on Computer Vision*, pages 7346–7356, 2023. [2](#)
- [10] Sicheng Gao, Xuhui Liu, Bohan Zeng, Sheng Xu, Yanjing Li, Xiaoyan Luo, Jianzhuang Liu, Xiantong Zhen, and Baochang Zhang. Implicit diffusion models for continuous super-resolution. In *Proceedings of the IEEE/CVF Conference on Computer Vision and Pattern Recognition*, pages 10021–10030, 2023. [2](#), [3](#), [8](#)
- [11] Jonathan Ho, Ajay Jain, and Pieter Abbeel. Denoising diffusion probabilistic models. *Advances in neural information processing systems*, 33:6840–6851, 2020. [2](#), [3](#), [6](#)
- [12] Jonathan Ho, Chitwan Saharia, William Chan, David J Fleet, Mohammad Norouzi, and Tim Salimans. Cascaded diffusion models for high fidelity image generation. *The Journal of Machine Learning Research*, 23(1):2249–2281, 2022. [2](#), [3](#)
- [13] Junjie Ke, Qifei Wang, Yilin Wang, Peyman Milanfar, and Feng Yang. Musiq: Multi-scale image quality transformer. In *Proceedings of the IEEE/CVF International Conference on Computer Vision*, pages 5148–5157, 2021. [7](#)
- [14] Diederik Kingma and Jimmy Ba. Adam: A method for stochastic optimization. *International Conference on Learning Representations*, 2014. [6](#)
- [15] Wei-Sheng Lai, Jia-Bin Huang, Oliver Wang, Eli Shechtman, Ersin Yumer, and Ming-Hsuan Yang. Learning blind video temporal consistency. In *Proceedings of the European conference on computer vision (ECCV)*, pages 170–185, 2018. [7](#)
- [16] Christian Ledig, Lucas Theis, Ferenc Huszár, Jose Caballero, Andrew Cunningham, Alejandro Acosta, Andrew Aitken, Alykhan Tejani, Johannes Totz, Zehan Wang, et al. Photo-realistic single image super-resolution using a generative adversarial network. In *Proceedings of the IEEE conference on computer vision and pattern recognition*, pages 4681–4690, 2017. [2](#)
- [17] Haoying Li, Yifan Yang, Meng Chang, Shiqi Chen, Huajun Feng, Zhihai Xu, Qi Li, and Yueting Chen. Srdiff: Single image super-resolution with diffusion probabilistic models. *Neurocomputing*, 479:47–59, 2022. [2](#), [3](#), [8](#)
- [18] Jingyun Liang, Jiezhong Cao, Yuchen Fan, Kai Zhang, Rakesh Ranjan, Yawei Li, Radu Timofte, and Luc Van Gool. Vrt: A video restoration transformer. *arXiv preprint arXiv:2201.12288*, 2022. [2](#), [6](#), [7](#)
- [19] Jingyun Liang, Yuchen Fan, Xiaoyu Xiang, Rakesh Ranjan, Eddy Ilg, Simon Green, Jiezhong Cao, Kai Zhang, Radu Timofte, and Luc V Gool. Recurrent video restoration transformer with guided deformable attention. *Advances in Neural Information Processing Systems*, 35:378–393, 2022. [1](#), [2](#), [6](#), [7](#)
- [20] Bee Lim, Sanghyun Son, Heewon Kim, Seungjun Nah, and Kyoung Mu Lee. Enhanced deep residual networks for single image super-resolution. In *Proceedings of the IEEE conference on computer vision and pattern recognition workshops*, pages 136–144, 2017. [8](#)
- [21] Hongying Liu, Zubo Ruan, Peng Zhao, Chao Dong, Fanhua Shang, Yuanyuan Liu, Linlin Yang, and Radu Timofte. Video super-resolution based on deep learning: a comprehensive survey. *Artificial Intelligence Review*, 55(8):5981–6035, 2022. [2](#), [8](#)
- [22] Zhengxiong Luo, Dayou Chen, Yingya Zhang, Yan Huang, Liang Wang, Yujun Shen, Deli Zhao, Jingren Zhou, and Tieniu Tan. Videofusion: Decomposed diffusion models for high-quality video generation. In *Proceedings of the IEEE/CVF Conference on Computer Vision and Pattern Recognition*, pages 10209–10218, 2023. [2](#), [4](#)

- [23] Anish Mittal, Rajiv Soundararajan, and Alan C Bovik. Making a “completely blind” image quality analyzer. *IEEE Signal processing letters*, 20(3):209–212, 2012. 7
- [24] Seungjun Nah, Sungyong Baik, Seokil Hong, Gyeongsik Moon, Sanghyun Son, Radu Timofte, and Kyoung Mu Lee. Ntire 2019 challenge on video deblurring and super-resolution: Dataset and study. In *Proceedings of the IEEE/CVF Conference on Computer Vision and Pattern Recognition Workshops*, pages 0–0, 2019. 6, 7, 1, 2
- [25] Robin Rombach, Andreas Blattmann, Dominik Lorenz, Patrick Esser, and Björn Ommer. High-resolution image synthesis with latent diffusion models. In *Proceedings of the IEEE/CVF conference on computer vision and pattern recognition*, pages 10684–10695, 2022. 2, 3, 4, 5, 6
- [26] Olaf Ronneberger, Philipp Fischer, and Thomas Brox. U-net: Convolutional networks for biomedical image segmentation. In *Medical Image Computing and Computer-Assisted Intervention–MICCAI 2015: 18th International Conference, Munich, Germany, October 5-9, 2015, Proceedings, Part III 18*, pages 234–241. Springer, 2015. 4, 8, 1
- [27] Claudio Rota, Marco Buzzelli, Simone Bianco, and Raimondo Schettini. Video restoration based on deep learning: a comprehensive survey. *Artificial Intelligence Review*, 56(6):5317–5364, 2023. 2, 3, 8
- [28] Hshmat Sahak, Daniel Watson, Chitwan Saharia, and David Fleet. Denoising diffusion probabilistic models for robust image super-resolution in the wild. *arXiv preprint arXiv:2302.07864*, 2023. 3
- [29] Chitwan Saharia, William Chan, Saurabh Saxena, Lala Li, Jay Whang, Emily L Denton, Kamyar Ghasemipour, Raphael Gontijo Lopes, Burcu Karagol Ayan, Tim Salimans, et al. Photorealistic text-to-image diffusion models with deep language understanding. *Advances in Neural Information Processing Systems*, 35:36479–36494, 2022. 2, 3
- [30] Chitwan Saharia, Jonathan Ho, William Chan, Tim Salimans, David J Fleet, and Mohammad Norouzi. Image super-resolution via iterative refinement. *IEEE Transactions on Pattern Analysis and Machine Intelligence*, 45(4):4713–4726, 2022. 2, 3, 8
- [31] Zachary Teed and Jia Deng. Raft: Recurrent all-pairs field transforms for optical flow. In *Computer Vision–ECCV 2020: 16th European Conference, Glasgow, UK, August 23–28, 2020, Proceedings, Part II 16*, pages 402–419. Springer, 2020. 6
- [32] Yapeng Tian, Yulun Zhang, Yun Fu, and Chenliang Xu. Tdan: Temporally-deformable alignment network for video super-resolution. In *Proceedings of the IEEE/CVF conference on computer vision and pattern recognition*, pages 3360–3369, 2020. 2, 6, 7
- [33] Ashish Vaswani, Noam Shazeer, Niki Parmar, Jakob Uszkoreit, Llion Jones, Aidan N Gomez, Łukasz Kaiser, and Illia Polosukhin. Attention is all you need. *Advances in neural information processing systems*, 30, 2017. 2
- [34] Jianyi Wang, Kelvin CK Chan, and Chen Change Loy. Exploring clip for assessing the look and feel of images. In *Proceedings of the AAAI Conference on Artificial Intelligence*, pages 2555–2563, 2023. 7
- [35] Xintao Wang, Kelvin CK Chan, Ke Yu, Chao Dong, and Chen Change Loy. Edvr: Video restoration with enhanced deformable convolutional networks. In *Proceedings of the IEEE/CVF conference on computer vision and pattern recognition workshops*, pages 0–0, 2019. 2, 6, 7
- [36] Zhou Wang, Alan C Bovik, Hamid R Sheikh, and Eero P Simoncelli. Image quality assessment: from error visibility to structural similarity. *IEEE transactions on image processing*, 13(4):600–612, 2004. 7
- [37] Tianfan Xue, Baian Chen, Jiajun Wu, Donglai Wei, and William T Freeman. Video enhancement with task-oriented flow. *International Journal of Computer Vision*, 127:1106–1125, 2019. 1, 2, 6, 7
- [38] Sihyun Yu, Kihyuk Sohn, Subin Kim, and Jinwoo Shin. Video probabilistic diffusion models in projected latent space. In *Proceedings of the IEEE/CVF Conference on Computer Vision and Pattern Recognition*, pages 18456–18466, 2023. 2, 5
- [39] Lvmin Zhang, Anyi Rao, and Maneesh Agrawala. Adding conditional control to text-to-image diffusion models. In *Proceedings of the IEEE/CVF International Conference on Computer Vision*, pages 3836–3847, 2023. 4, 5, 6, 1
- [40] Richard Zhang, Phillip Isola, Alexei A Efros, Eli Shechtman, and Oliver Wang. The unreasonable effectiveness of deep features as a perceptual metric. In *Proceedings of the IEEE conference on computer vision and pattern recognition*, pages 586–595, 2018. 1, 2, 7
- [41] Hongkai Zheng, Weili Nie, Arash Vahdat, Kamyar Azizzadenesheli, and Anima Anandkumar. Fast sampling of diffusion models via operator learning. In *International Conference on Machine Learning*, pages 42390–42402. PMLR, 2023. 8
- [42] Xizhou Zhu, Han Hu, Stephen Lin, and Jifeng Dai. Deformable convnets v2: More deformable, better results. In *Proceedings of the IEEE/CVF conference on computer vision and pattern recognition*, pages 9308–9316, 2019. 2

Enhancing Perceptual Quality in Video Super-Resolution through Temporally-Consistent Detail Synthesis using Diffusion Models

Supplementary Material

Table 3. Architectural details of StableVSR.

	Denoising UNet	Temporal Conditioning Module	VAE decoder
Downscaling	$\times 8$	$\times 8$	-
Upscaling	$\times 8$	-	$\times 4$
Input channels	7	3	4
Output channels	4	-	3
Trainable	No	Yes	No
Parameters	473 M	207 M	32 M

8. Additional experiments

8.1. Additional implementation details

We report the StableVSR architecture details in Table 3. Following ControlNet [39], we freeze the weights of the Denoising UNet [26] during training. We only train the Temporal Conditioning Module (TCM) for video adaptation. We apply spatial guidance on the low-resolution frame via concatenation, i.e. the noisy latent x_t^i (4 channels) is directly concatenated with the low-resolution frame LR^i (3 channels). The temporal guidance is instead provided via TCM, which receives Temporal Texture Guidance $\widetilde{HR}^{i-1 \rightarrow i}$ as input (3 channels). The VAE decoder \mathcal{D} [8] receives the final latent, i.e. x_0^i , of a frame i as input, and converts it into an RGB frame. This latent-to-RGB conversion applies $\times 4$ upscaling, hence the output of the decoder represents the upscaled frame. The overall number of parameters in StableVSR (including the VAE decoder [8]) is about 712 million.

8.2. Additional ablation study

Temporal Texture Guidance. We extend the ablation study on Temporal Texture Guidance by reporting the quantitative results on the ablated components in Table 4. Without using the guidance on \tilde{x}_0 (“No guidance on \tilde{x}_0 ” row), i.e. directly using x_t , a strong temporal inconsistency is introduced. The lack of proper mechanisms for spatial alignment, such as in the case of no motion compensation (“No MC” row) or motion compensation in the VAE latent space [8] (“No Latent \rightarrow RGB conversion” row), limits the overall frame quality and temporal consistency. In comparison, the proposed Temporal Texture Guidance, which includes all the aforementioned operations, leads to better quality and temporal consistency. Figure 9 shows that only the proposed Temporal Texture Guidance ensures temporal consistency at the fine-detail level over time.

Table 4. Additional ablation experiments for Temporal Texture Guidance, quantitative results. Perceptual metrics are marked with \star , reconstruction metrics with \diamond , and temporal consistency metrics with \bullet . Best results in bold text. We also report single-image results as the baseline. The proposed Temporal Texture Guidance leads to significant improvements in temporal consistency. MC refers to “motion compensation”. For “No guidance on \tilde{x}_0 ” experiment, we use guidance on x_t . Results computed on center crops of 512×512 target resolution of REDS [24].

	WE \bullet \downarrow	LPIPS \star \downarrow	DISTS \star \downarrow	PSNR \diamond \uparrow	SSIM \diamond \uparrow
Baseline (single-image)	2.44	0.121	0.055	26.32	0.732
No guidance on \tilde{x}_0	3.11	0.135	0.065	25.69	0.706
No motion compensation	2.51	0.116	0.051	26.61	0.751
No Latent \rightarrow RGB conv.	2.46	0.113	0.500	26.65	0.753
Proposed	1.51	0.097	0.045	27.97	0.800

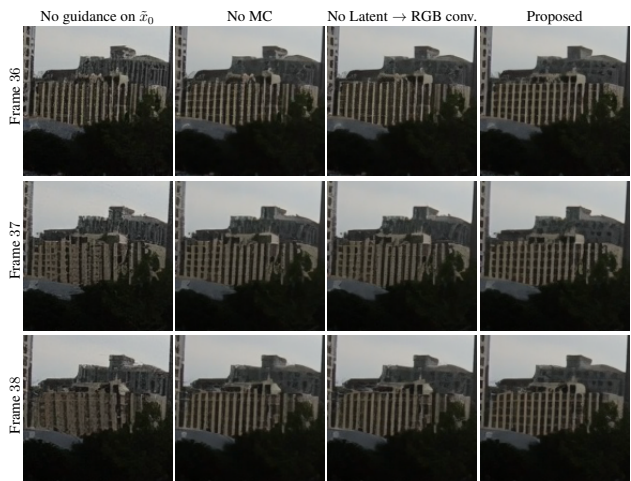


Figure 9. Additional ablation experiments for the Temporal Texture Guidance. We show the results obtained on three consecutive frames. Only the proposed solution ensures temporal consistency at the fine-detail level over time. Results on sequence 015 of REDS [24].

8.3. Additional comparison with the state-of-the-art

Figure 10 shows an additional qualitative comparison with state-of-the-art methods on Vimeo90K [37] (Figure 10a) and REDS [24] (Figure 10b). We can observe StableVSR is the only method that correctly upscales complex textures while the other methods fail, producing blurry details.



(a) Results on Vimeo90k [37].



(b) Results on REDS [24].

Figure 10. Additional qualitative comparison with state-of-the-art methods. Our results are shown in the last column (StableVSR).